Published in final edited form as:
Biomaterials. 2011 March ; 32(8): 2183–2193. doi:10.1016/j.biomaterials.2010.11.040.

Polyethylene Glycol Modified, Cross-Linked Starch Coated Iron Oxide Nanoparticles for Enhanced Magnetic Tumor Targeting

Adam J. Cole[1], **Allan E. David**[1,3], **Jianxin Wang**[1,4], **Craig J. Galbán**[2], **Hannah L. Hill**[1], and **Victor C. Yang**[1,5,*]

[1] Department of Pharmaceutical Sciences, College of Pharmacy, University of Michigan, Ann Arbor, Michigan 48109-1065, USA

[2] Department of Radiology, Center for Molecular Imaging, Medical School, University of Michigan, Ann Arbor, Michigan 48109-2200, USA

[3] Industrial Science & Technology Network Inc., York, PA 17404, USA

[4] Department of Pharmaceutics, School of Pharmacy, Fudan University, Shanghai 201203, China

[5] Tianjin Key Laboratory for Modern Drug Delivery and High Efficiency, Tianjin University, Tianjin 300072, China

Abstract

While successful magnetic tumor targeting of iron oxide nanoparticles has been achieved in a number of models, the rapid blood clearance of magnetically suitable particles by the reticuloendothelial system (RES) limits their availability for targeting. This work aimed to develop a long-circulating magnetic iron oxide nanoparticle (MNP) platform capable of sustained tumor exposure via the circulation and, thus, enhanced magnetic tumor targeting. Aminated, cross-linked starch (DN) and aminosilane (A) coated MNPs were successfully modified with 5 kDa (A5, D5) or 20 kDa (A20, D20) polyethylene glycol (PEG) chains using simple N-Hydroxysuccinimide (NHS) chemistry and characterized. Identical PEG-weight analogues between platforms (A5 & D5, A20 & D20) were similar in size (140–190 nm) and relative PEG labeling (1.5% of surface amines – A5/D5, 0.4% – A20/D20), with all PEG-MNPs possessing magnetization properties suitable for magnetic targeting. Candidate PEG-MNPs were studied in RES simulations *in vitro* to predict long-circulating character. D5 and D20 performed best showing sustained size stability in cell culture medium at 37°C and 7 (D20) to 10 (D5) fold less uptake in RAW264.7 macrophages when compared to previously targeted, unmodified starch MNPs (D). Observations *in vitro* were validated *in vivo*, with D5 (7.29 hr) and D20 (11.75 hr) showing much longer half-lives than D (0.12 hr). Improved plasma stability enhanced tumor MNP exposure 100 (D5) to 150 (D20) fold as measured by plasma $AUC_{0-\infty}$ Sustained tumor exposure over 24 hours was visually confirmed in a 9L-glioma rat model (12 mg Fe/kg) using magnetic resonance imaging (MRI). Findings indicate that both D5 and D20 are promising MNP platforms for enhanced magnetic tumor targeting, warranting further study in tumor models.

*Correspondence and reprint request should be addressed to: Victor C. Yang, Ph.D., Albert B. Prescott Professor of Pharmaceutical Sciences, College of Pharmacy, University of Michigan, 428 Church Street, Ann Arbor, Michigan 48109-1065, Tel: (734)764–4273, Fax: (734)763–9772, vcyang@umich.edu.

Keywords

iron oxide nanoparticles; magnetic nanoparticles; magnetic targeting; polyethylene glycol (PEG); pharmacokinetics; reticuloendothelial system (RES); drug delivery; brain tumor; glioma

1. INTRODUCTION

Magnetic iron oxide nanoparticles (MNP) have been widely explored for use in biomedical applications, including cancer therapy [1]. MNPs typically consist of a superparamagnetic iron oxide (usually Fe_3O_4 or γ-Fe_2O_3) core coated with a "shell" that exhibits good biocompatibility. Shells are usually polymeric (e.g. synthetic polymers, polysaccharides) in nature, but can also consist of proteins, lipids, or smaller organic chains often linked to nanoparticle cores via silica [2]. Considered potential "theranostics", MNPs have been utilized in both diagnostic and therapeutic applications in oncology [3]. Diagnostically, the T_2/T_2* proton relaxation properties of MNPs have been exploited for their use as contrast enhancement agents in magnetic resonance imaging (MRI) [4]. Often in conjunction with MRI, tumor therapy modalities have also been investigated and include magnetically induced hyperthermia treatments [5] and/or the delivery of anti-neoplastic agents [3,6,7]. The large surface area-to-volume ratio characteristic of nanoparticles renders the MNP an excellent candidate for drug loading and transport. Moreover, MNPs are passively targeted to solid tumors by the enhanced permeability and retention (EPR) effect, whereby carriers up to 1 μm have been shown to passively extravasate through compromised tumor vasculature and into its interstitium [8]. Additional accumulation enhancements can be realized actively with tumor-targeted ligands (e.g. small molecules, peptides, antibodies, other proteins) [7,9–11] and/or the application of an external magnetic field to tumor regions [1,12]. Indeed, enhanced tumor accumulation of MNPs after magnetic targeting has been confirmed in a number of cancer models, including brain [12–15].

The success of magnetic targeting is highly dependent on MNP physiochemical properties, the strength of the applied magnetic force, and nanoparticle pharmacokinetics. Tumor capture of MNPs occurs when the magnetic force is sufficient to overcome drag forces associated with convective blood flow – the stronger the magnetic force, the greater the retention. The magnetic force strength on a MNP is a function of the magnetic field gradient (∇B) generated by the applied field (B); the core material's magnetic susceptibility (χ_χ); and the core volume (V_c) as shown in Equation 1 [12]:

$$F_{MNP} = \frac{\chi_c V_c}{\mu_0} B(\nabla B) \quad (1)$$

where μ_0 is the magnetic permeability of free space. The gradient is a function of the field strength and its geometry, while the magnetic susceptibility is a constant material property of the specific iron oxide comprising the MNP core. Given fixed field geometry and core material properties, the nanoparticle core size (volume) is the only *adjustable* parameter available to modulate the capture force and, thus, tumor MNP retention. Equation 1 suggests that larger-core MNPs (>100 nm) are preferred, especially where the magnetic gradient is weak (e.g. deep tumors some distance away from the field source). A critical diameter threshold (on the order of ~10–30 nm) for iron-oxide domains comprising the core, however, must be met to retain superparamagnetism of the MNP – an important property that prevents unwanted self-aggregation of MNPs in the absence of the applied field [1]. Therefore, the cores of MNPs used in conjunction with magnetic targeting typically consist of multiple, smaller iron-oxide domains, rather than a single, larger domain [13–15]. While a

multi-domain structure allows for larger cores, the potential for microvessel embolism places an upper constraint on overall particle size (including core diameter), thus, limiting potential magnetic targeting force [16]. Considering limits on force due to limits on the applied field and particle size, strategies to extend the targeting availability (tumor exposure) of MNPs should also be explored.

The circulation half-lives of MNPs preferred for magnetic targeting are fairly short (on the order of minutes) due to quick opsonization of MNPs and subsequent plasma clearance by tissue macrophages of the reticuloendothelial system (RES) [15,17,18]. Both passive and active forms of targeting (including magnetic targeting) require presentation of MNPs to the tumor via the circulation. Fast clearance effects of larger MNPs favored for magnetic targeting, though, reduce the exposure of tumors to MNP thereby limiting their availability for interaction with the applied magnetic field. While reducing particle size can extend circulation time, smaller MNPs (< 100 nm) could be difficult to magnetically target considering Equation 1 [19]. Additional interventions such as intra-arterial injections (to avoid first pass clearance) and temporary disruption of bioprotective structures have been explored with magnetic targeting to overcome pharmacokinetic limitations [15,17,19]. These methods, while promising, add another layer of complexity to treatments and, thus, could be clinically challenging. Polyethylene glycol (PEG), a classic pharmacokinetic stabilizer, has been utilized to extend MNP circulations times *in vivo*, but almost exclusively for MNPs too small (< 100 nm, often comprised of single domain cores < 20 nm) to be sufficiently targeted [4,11,20–24]. Much to our surprise, the literature contains few reports of a MNP primed for magnetic targeting (> 100 nm, multi-domain core) *and* shown to be sufficiently long circulating *in vivo*.

Intending to overcome the pharmacokinetic limitations attributed to traditionally fast clearance, this work aimed to produce long-circulating MNPs adequate for enhanced magnetic tumor targeting. To that end, we modified two commercially available MNP platforms (based on silica and starch coatings, respectively) with PEG utilizing simple, aqueous phase synthesis procedures. Candidate PEG-MNPs were fully characterized *in vitro* for both their physical properties and potential to evade RES elements *in vivo*. Promising candidates *in vitro* were then passed to *in vivo* plasma pharmacokinetic studies in rats to validate their performance. MR images of a 9L-glioma rat model were used to visually confirm sustained exposure of long-circulating PEG-MNPs to tumors.

2. MATERIALS AND METHODS

2.1. Materials

All materials were purchased from commercial suppliers and used without further modification, unless otherwise noted. fluidMAG-D (“D”, starch coated magnetite iron-oxide nanoparticles, coating shown in Figure 1A) and fluidMAG-Amino (“A”, aminosilane coated magnetite iron-oxide nanoparticles, coating shown in Figure 1A) both at 75 mg/mL were obtained from Chemicell® GmbH (Berlin, Germany). Methoxyl polyethylene glycol succinimidyl carbonates (SC NHS-PEG) in 5 and 20 kDa molecular weights were obtained from Nanocs (New York, NY). Ninhydrin reagent (2%), 0.1 N iodine solution, dimethylsulfxodide (DMSO), QuantiPro BCA Assay kit (containing 4% copper (II) sulfate pentahydrate solution, QuantiPro Buffer QA, and QuantiPro BCA QB, and bovine serum albumin (BSA) standard), 4-(2-Hydroxyethyl)piperazine-1-ethanesulfonic acid, N-(2-Hydroxyethyl)piperazine-N′-(2-ethanesulfonic acid) (HEPES), sodium phosphate (mono- and di-basic), 37% hydrochloric acid (HCl), epichlorohydrin, concentrated ammonium hydroxide (NH_4OH, containing 30% ammonia), sodium hydroxide (NaOH), spectroscopic grade potassium bromide (KBr), sodium chloride (NaCl), and sodium dodecyl sulfate (SDS) were obtained from Sigma-Aldrich (St. Louis, MO). 10% (w/v) barium chloride ($BaCl_2$)

solution was obtained from Ricca Chemical (Arlington, TX). RPMI Medium 1640 (supplemented with glutamine, containing phenol red), Dulbecco's Modified Eagle Medium (DMEM – supplemented with L-glutamine and sodium pyruvate), antibiotics, fetal bovine serum (FBS), cell culture grade phosphate buffered saline (PBS—1X–pH 7.4), and 0.25% trypsin-EDTA were obtained from Invitrogen (Carlsbad, CA). Deinoized water (DI H_2O) used throughout the study was obtained from a Milli-Q A10 Biocel water purification system (Millipore, Billerica, MA). Murine RAW264.7 macrophage cell line was purchased from ATCC (Manassas, VA). Rat 9L gliosarcoma cell line was obtained from the Brain Tumor Research Center (University of California, San Francisco, CA). Sterile heparin solutions (10 U/mL and 5000 U/mL) (Abraxis, Los Angeles, CA) were obtained from the University of Michigan Hospital Pharmacy.

2.2. Synthesis of iron oxide nanoparticles

Throughout the course of syntheses, iron content in MNP preparations was measured by inductively coupled optical emission (ICP-OES) spectroscopy using an Optima DV 2000 spectrometer (Perkin Elmer, Waltham, MA) as described previously [25]. Briefly, 10 μL of diluted MNP solution was digested in 2 mL concentrated hydrochloric acid and brought to 5 mL total volume with DI H_2O to an iron concentration of 1–5 mg Fe/L. Samples were analyzed in triplicate at 238.204 nm. The instrument was calibrated using dilutions of an iron standard (0–10 mg Fe/L) in DI H_2O spiked with a yittrium internal standard (1 mg Fe/L, GFS Chemicals, Columbus, OH).

2.2.1. Cross-linked, aminated starch MNP (DN)—As shown in Figure 1B, starch moieties on D MNPs were cross-linked and aminated by adapting methodology previously developed for dextran coated MNPs [26, 27]. 2 mL of D (42 mg Fe/mL) suspension were incubated with 2.6 mL NaOH for 15 min. 1.3 mL of epichlorohydrin was then added to the mixture and incubated for 24 hr at 25°C with shaking. The c ross-linked product (DXL) was then dialyzed extensively against DI H_2O using a 10,000 MWCO Slide-A-Lyzer dialysis cassette (Thermo Scientific, Rockford, IL). The purified DXL product (~12 mL) was then incubated with 2 mL of concentrated NH_4OH (30% ammonia) for 24 hr at 25°C with shaking. The cross-linked, aminated product (DN) was then dialyzed extensively against DI H_2O using a 10,000 MWCO Slide-A-Lyzer dialysis cassette. After purification, DN was concentrated using a Dynal magnetic separator (Invitrogen, Carlsbad, CA) to 30–40 mg Fe/mL.

2.2.2. Aminosilane based polyethylene glycol (PEG) MNPs (A5 & A20)—As shown in Figure 1C, A-based PEG-MNPs were synthesized in simple fashion using *N*-Hydroxysuccinimide (NHS) chemistry. 320 μL of A (40 mg Fe/mL) were added to 640 μL pH 7 0.1 M HEPES buffer containing ~30 mg dissolved SC-PEG-NHS (5 kDa or 20 kDa MW). The mixture was incubated at 25°C with shaking for 3 hr. At the completion of the synthesis, the reaction mixture was diluted to 7 mL. Small aggregates were dispersed with 2 min of sonication using a Sonifier sonicator operated at 10% amplitude (Branson, Danbury, CT) at 25°C. The sonicated solution was then placed on a Dynal magnetic separator and washed 4 times with fresh DI H_2O. After the final wash, the purified product (A5 or A20 containing 5 kDa or 20 kDa PEG respectively) was concentrated to 40 mg Fe/mL.

2.2.3. Starch based polyethylene glycol (PEG) MNPs (D5 & D20)—As shown in Figure 1C, D-based PEG-MNPs were also synthesized using NHS chemistry. 320 μL of A (30 mg Fe/mL) were added to a mixture of 320 μL DMSO and 320 μL (640 μL for 20 kDa analogue) pH 8 0.1 M phosphate buffer containing ~30 mg dissolved SC-PEG-NHS (5 kDa or 20 kDa MW). The mixture was incubated at 25°C with shaking for 3 hr. At the completion of the synthesis, the reaction mixture was diluted to 7 mL, placed on a Dynal

magnetic separator, and washed 4 times with fresh DI H_2O. Particle size was controlled with sonication using a Sonifier sonicator operated at 10% amplitude at 25°C. After the final wash, the purified product (D5 or D20 containing 5 kDa or 20 kDa PEG respectively) was concentrated to 40 mg Fe/mL.

2.3. Characterization of MNPs

Z-average, intensity-weighted size (hydrodynamic diameter) distribution and zeta potential measurements were measured by dynamic light scattering (DLS). Measurements were taken in triplicate from very dilute MNP suspensions (1 mL) in DI H_2O using a ZetaSizer Nano ZS90 particle-sizing instrument (Malvern, Worcestershire, UK). A standard ninhydrin assay was used to quantitatively characterize the amine content of A and DN by measuring the amine-initiated production of Ruhemann's Purple at 570 nm [15,28]. To characterize levels of PEG on PEG-MNPs, an adapted barium iodide assay was used [29]. Briefly, 50 μL of MNP dispersion was digested in 100 μL 12 M HCl and then diluted with 100 μL DI H_2O. 50 μL of this solution was then added to 100 μL 1% (w/v) $BaCl_2$ in a 96-well plate. Immediately prior to spectrophotometric measurements, 100 μL of 0.001 N iodine solution was added to the MNP/$BaCl_2$ mixture. Samples were allowed to react for 30 min and then measured at 535 nm. Calibration curves were constructed using the appropriate SC-NHS-PEG (5 kDa or 20 kDa). All spectrophotometric analyses were completed in triplicate using a PowerWaveX340 spectrophotometer (Biotek, Winooski, VT).

Fourier transform infrared spectroscopy (FTIR) was used to collect infrared spectra (IR) from lyophilized MNP samples. 2–3 mg MNP powder was mixed and ground with 100–150 mg spectroscopic grade KBr and pressed into ~1 mm thick discs. IR spectra were recorded using a Spectrum BX FTIR spectrometer (Perkin Elmer, Waltham, MA). Transmission electron microscopy (TEM) was conducted using a JEOL 3011 high-resolution electron microscope (Tokyo, Japan) operated at an accelerated voltage of 300 kV. Samples were prepared by applying very dilute MNP dispersions to 01813-F formvar-coated copper grids (Ted Pella, Redding, CA) with a pipette followed by ambient drying. Magnetization properties of MNP solutions were assessed using a MPMS-XL Superconducting Quantum Interference Device (SQUID) magnetometer (Quantum Design, San Diego, CA). Fluid samples were mounted in capsules and analyzed at varying DC magnetic field (0–15000 G) at 25°C in both increasing and decreasing field directions.

2.4. *In vitro* reticuloendothelial system (RES) resistance simulations and stability

2.4.1 Protein binding study—Protein binding studies were conducted using a modified protocol to that described elsewhere [30]. Briefly, MNP suspensions were diluted with DI H_2O to 4.0 mg Fe/mL. 100 μL of diluted MNP suspension was then added to 100 μL 10 mM PBS (pH 7.4) and 300 μL FBS (n = 6). Samples were incubated for 2 hr at 37°C. Following incubations, samples were centrifug ed at 15000 × g for 20 min and washed 5 times (with centrifugation) with 1 mL fresh 10 mM PBS (pH 7.4). 900 μL of the final wash volume was removed and 150 μL 5% SDS in PBS was added to the mixture and incubated for 10 min to removed bound protein from MNPs. Following centrifugation at 15000 × g for 20 min, 150 μL of supernatant was mixed with 150 μL bicinchoninic acid (BCA) reagent (2.5 mL QA buffer + 2.5 mL QB buffer + 0.1 mL 4% copper (II) sulfate pentahydrate solution) and heated for 1 hour at 60°C. After heating, a 150 μL aliquot was withdrawn for spectrophotometric analysis at 562 nm. Bovine serum albumin (BSA) was used as a protein standard for calibration curves. D, used in previous magnetic targeting studies, was used as a benchmark in comparing results [14,15,25]. A was not considered for comparisons, as its aminated surface would likely result in its rapid clearance *in vivo* [15].

2.4.2 Particle size stability in RAW264.7 macrophage cell culture medium— MNPs were dispersed in 1 mL complete RAW264.7 macrophage culture medium (RPMI medium 1640 containing 10% FBS, and 1% antibiotics) at a concentration of 0.1 mg Fe/mL. Samples were first inspected visually for large aggregates—MNPs exhibiting intense aggregation were not studied further. Samples without noticeable aggregation were incubated in triplicate over 24 hr at 37°C. At set time points, 100 μL aliquots were removed for particle size analysis by DLS as described in Section 2.3.

2.4.3 RAW264.7 macrophage uptake study—MNP uptake in macrophages was studied using a modified protocol to that established previously [31]. Briefly, RAW264.7 cells were cultured in 100 mm dishes containing RPMI 1640 supplemented with 10% FBS and 1% antibiotics at 37°C in a humidified atmosphere of 5% CO_2. Cells were harvested with a cell scraper, counted with a hemocytometer, and seeded at approximately 1.125×10^5 cells/well in 12-well cell culture plate. Plates were incubated overnight in 1 mL culture medium under conditions described above to allow cells to attach and grow to ~70% confluence. Seeding medium was replaced with 1 mL complete culture medium containing MNP suspension (0.1 mg Fe/mL, n = 6) and allowed to incubate for 4 hr at 37°C as described above. In cubations with blank culture media (no MNP) were used as a control. Incubation media containing MNPs was then removed and the cells were washed 3 times with serum and antibiotic free RPMI 1640. 350 μL of cell culture grade 1× PBS (pH 7.4) was then added and the cells subsequently detached from the culture plate by scraping. 100 μL of cell suspension was added to electron spin resonance (ESR) tubes using a microsyringe attached to a 12 in. Teflon needle. Samples were stored at −80°C prior to quantitative ESR analysis described in Section 2.6. Again, D was used as a benchmark for studies.

2.5. Validating long-circulating properties of D5 and D20 *in vivo*

All animal experiments were conducted according to protocols reviewed and approved by the University of Michigan Committee on Use and Care of Animals (UCUCA).

2.5.1. Plasma pharmacokinetic analyses of D, D5, and D20—Male Fisher 344 rats (~200 g, Harlan, Indianapolis, IN) were anesthetized by intraperitoneal injection of ketamine/xylazine mixture (87/13 mg/kg BW). The lateral tail vein was cannulated with a 26-gauge Angiocath™ catheter (Hospira, Lake Forrest, IL) and flushed briefly with 10 U/mL heparin lock solution. MNP suspensions were diluted to 10.25 mg Fe/mL in 1× cell culture grade PBS (pH 7.4) and administered through the catheter at a dose of 12 mg Fe/kg, consistent with previous magnetic targeting studies [14,15]. Blood collection was performed using two different routes depending on the expected clearance of the MNP from the circulation. D previously showed fast clearance from plasma (half-life on the order of minutes), and, thus, blood samples were taken from a cannula inserted into the left carotid artery – a route good for rapid sample withdrawal [15]. Briefly, the left carotid artery was isolated using blunt, curved hemostats, carefully separated from the vagus nerve, ligated rostrally with silk sutures, and temporarily clipped caudally to prevent blood flow. A small incision in the artery wall was made with microscissors and subsequently catheterized with PE-10 tubing, with the cannula held in place with silk sutures. The caudal artery clip was removed to perfuse the cannula, which was then flushed with 10 U/mL heparin lock solution. 100 μL blood samples were collected at rapid time points over 1 hr into 0.5 mL tubes spiked with 10 μL 5000 U/mL heparin solution. Samples were immediately centrifuged at 500 × g for 3 min to separate the plasma from whole blood. 30 μL of plasma was added to an ESR tube using a microsyringe attached to a 12 in. Teflon syringe needle and stored at −80°C prior to quantitative analysis described in Section 2.6. Since carotid sampling required opening the body cavity, catheterizing the carotid artery, and sustaining

anesthesia, it was not considered a viable sampling route for PEG-MNPs expected to clear over the course of days. Therefore, D5 and D20 studies were completed by venipuncture of the lateral tail vein at set time points. Longer gaps between collections times helped minimize sampling variability. 100 μL of beaded blood was collected into 0.5 mL, heparin-spiked tubes for further analysis as described in Section 2.6. To prevent vein collapse from excessive tail sticks, sampling was taken at time points from two sets (0–12 hours, 12–60 hours, n = 3 per set) of animals. D was studied for comparison with D5 and D20 profiles.

For each MNP analyzed, a one-compartment pharmacokinetic model was constructed from experimental plasma data using non-linear regression according to equation 2:

$$C(t)=C_0e^{-kt} \tag{2}$$

where C_0 is the initial plasma MNP concentration, $C(t)$ is the plasma MNP concentration at time t, and k is the elimination rate constant. Half-life ($T_{1/2}$) was calculated according to equation 3. Body weight (BW)-normalized volume of distribution (V_d) was calculated according to equation 4 and used to calculate clearance (CL) according to equation 5. Additionally, total expected plasma MNP exposure per single dose was inferred from pharmacokinetic models by calculating the total area-under-the-curve ($AUC_{0\text{-}\infty}$) according to equation 6.

$$T_{1/2}=\frac{\ln(2)}{k} \tag{3}$$

$$V_d=\frac{Dose}{C_0 * BW} \tag{4}$$

$$CL=kV_d \tag{5}$$

$$AUC_{0-\infty}=\int_0^\infty C(t)dt \tag{6}$$

2.5.2. Induction of brain tumors—Intracerebral brain tumors were implanted in male Fisher 344 (125–150 g) rats as previously described [32]. Briefly, 9L glioma cells were cultured in T75 culture flasks to confluence in DMEM medium containing 10% heat inactivated FBS, 1% antibiotics, and 0.29 mg L-glutamine at 37°C in a humidified atmosphere containing 5% CO_2. Immediately preceding tumor implantation, cells were harvested using 0.25% trypsin-EDTA, washed with serum free medium, and each flask of cells resuspended in 1.3 mL serum free medium to a concentration of ~1×10^4 cells/μL. Animals were anesthetized by intraperitoneal injection of ketamine/xylazine mixture as described in Section 2.5.1. After making a small skin incision over the right hemisphere of the skull, a 1-mm-diameter burr hole was drilled into the skull approximately 1 mm anterior to the bregma and 5 mm lateral from the midline. 10 μL of 9L cell suspension was injected into the burr hole at a depth of 3–4 mm beneath the skull. The surgical field was cleaned several times with 100% ethanol and the burr hole sealed with bone wax (Ethicon, Summerfield, NJ) to prevent extracerebral extension of the tumor. The surgical site was

cleaned with iodine surgical scrub and the incision closed with Vetbond tissue adhesive (3M, St. Paul, MN). Animals were imaged every two days using a fast spin echo T_2-weighted MRI (see Section 2.5.3) sequence starting 11 days after tumor induction to select tumors between 50–100 μL in volume. Tumor volumes were assessed with in-house developed software using sizing methods previously described [32].

2.5.3. *in vivo* magnetic resonance imaging (MRI) monitoring of MNP tumor exposure in rat 9L-glioma model—Animals induced with brain tumors in Section 2.5.2. were injected with MNP suspensions (12 mg Fe/kg) once MRI scans showed a tumor volume of 50–100 μL (~180–210 g BW). Animals were anesthetized by intraperitoneal injection of ketamine/xylazine and tail vein catheterized as described in 2.6.2 for injections, and then imaged at set time points. MRI experiments were conducted as previously described, with modification [15]. Images were acquired on a 30-cm horizontal-bore, 7T Direct Drive small animal imaging system (Varian, Palo Alto, CA). Animals were anesthetized through inhalation of a 1.5% isoflurane/air mixture and imaged using a rat head quadrature RF coil (m2m Imaging, Cleveland, OH). Tumor was visualized within the brain prior to MNP administration using a high resolution T_2-weighted fast spin echo sequence with the following parameters: repetition time (TR) = 4000 ms, echo time (TE) = 60 ms, field of view 30 × 30 over 256 × 128 matrix, slice thickness = 1 mm, slice separation = 0 mm, number of slices = 15, and two signal averages. To visualize, dynamically, MNP presence in the brain and tumor, MR images were acquired using a gradient echo (GE) sequence prior to and at 1 hr, 5, hr, and 24 hr subsequent to MNP administration. The parameters used for the GE sequences were: TR = 180 ms, TE = 5 ms, flip angle = 20 deg, field of view = 30 × 30 over 128 × 128 matrix, slice thickness = 1 mm, slice separation = 0 mm, number of slices = 15, and one signal average. Baseline T_2-weighted and GE images were taken sequentially (without animal repositioning). The T_2-weighted slice showing the best cross-sectional view of the tumor at baseline was used to select corresponding GE images at imaged time points. Animals were repositioned in the magnet between imaging time points, with the chosen slices in Figure 6 matching as close as possible in position to the optimal T_2-weighted slice taken at baseline. MR images of tumor-bearing rats administered with D were obtained for comparison purposes.

2.6 Quantitative MNP analyses with ESR

Quantitative MNP analysis of RAW264.7 (Section 2.4.3) and plasma samples (Section 2.5.1.) was conducted using ESR as described previously [25]. Briefly, ESR spectra were acquired using an EMX ESR spectrometer (Bruker, Billerica, MA) set with the following parameters: resonant frequency = ~9.2 GHz; microwave power = 20 mW; and temperature = −128°C°. The combination of receiver gain (5×10^3 or 5×10^4) and modulation amplitude (1G or 5G) varied depending on both the type of sample and observed spectra intensity. Calibration standards were prepared by applying dilutions of known-iron-concentration MNP stock to the bottom of ESR tubes with a microsyringe coupled to a 12 in Teflon needle. Typical of ESR spectrometers, spectra were obtained as the first derivative (dP/dB) of absorbed microwave power (P) vs. the applied magnetic field (B). It is widely known that the double integral (DI) of collected spectra ($\int\int (dP/dB)dBdB$) is proportional to the number of resonating electronic spins in a measured sample. DI values were obtained from spectra using WinEPR software (Bruker, Billerica, MA). Control (no exposure to MNP) macrophage and plasma samples showed negligible DI when compared to test samples and, therefore, background correction was not necessary.

2.7. Statistical analysis

All data are presented as mean ± standard deviation (SD) unless otherwise noted. Statistical comparisons in *in vitro* simulations and *in vivo* validation studies were made using the

Student's *t* test with a significance of $p < 0.05$. Non-linear regression analysis of pharmacokinetic data was performed using Excel (Microsoft, Redmond, WA).

3. RESULTS

3.1. Synthesis of aminated-precursor DN; characterization of DN and A

Two different MNP platforms based on starch or silane surface coating were chosen to synthesize sets of candidate PEG-MNPs. Silica-based coatings have been used in a variety of syntheses to link PEG to MNPs [21,33–35] and were, thus, considered as a platform for this study. Specifically, an aminosilane-coated MNP (A) was chosen because it possesses amine functionality that could be easily exploited for additional modification. As shown in Figure 1A, the aminosilane coating more or less directly links its amine groups (and, thus, any attached cargo) to the surface of the MNP core via a small silica linker. As a second candidate platform, a macromolecular, polysaccharide starch-coated (shown in Figure 1A) MNP (D) was explored. Starch-coated MNPs have been shown useful in previous studies using magnetic targeting [13–15,17,25,36] and provide hydroxyl functional groups for additional conjugations. To ensure that the D was functionally similar to A, D was cross-linked with epichlorohydrin to covalently strengthen the starch coating and subsequently aminated with concentrated ammonia to form DN as shown in Figure 1B. DN and A were assessed for particle size distribution, surface charge characteristics, and amine content. As shown in Table 1, A possessed an average hydrodynamic diameter of 114 ± 1.2 nm. Cross-linking and amination of D (104.1 ± 2.3 nm) resulted in a small increase in average hydrodynamic diameter for DN to 134.3 ± 2.1 nm. Polydispersity indexes (PDI) were all low (< 0.2) indicating mono-modal size distributions. Zeta potential (in DI H_2O) results in Table 1 suggest successful amination of D to DN by the strong, expected positive shift in zeta potential from +9.0 ± 0.8 mV to +58.9 ± 0.6 mV, similar to that determined for A (+54.6 ± 0.8 mV). Based on the observed presence of Ruhemann's Purple after synthesis, ninhydrin data confirm successful amination of D to DN, which contained similar amine content to A (293 ± 32 nmol/mg Fe vs. 329 ± 29 nmol/mg Fe, respectively). Given the data in Table 1, A and DN precursors were considered functionally and colloidally similar.

3.2. Synthesis and characterization of candidate PEG-MNPs

NHS chemistry was used to synthesize 5 kDa and 20 kDa PEG-containing MNPs from both A and DN aminated precursors as shown in Figure 1C. Succinimidyl carbonate (SC) ester was chosen for syntheses as it possess substantially greater aqueous hydrolysis half-life (20.4 min) than more commonly sold succinimidyl carboxylmethyl (SCM) ester (0.75 min) [37]. As shown in Table 2, average hydrodynamic diameter increased slightly with increasing PEG chain length. D5 (142.2 ± 5.6 nm) and D20 (168.5 ± 1.4) were slightly smaller than their respective A5 (151.5 ± 1.6 nm) and A20 (190.0 ± 5.8 nm) counterparts. PDI values remained low, suggesting that PEG-MNPs remained mono-modally distributed. TEM images shown in Figure 2 generally confirm sizing results from DLS and show that the morphology (larger coated cores comprised of multiple smaller iron-oxide domains) of MNPs was conserved throughout synthesis steps. Displayed in Table 2, expected zeta potential (in DI H_2O) shifts toward neutral (from ~+55 mV to ~+25 mV) were observed for all candidate PEG-MNPs suggesting successful grafting of PEG to respective coatings.

Moreover, FTIR spectra in Figure 3A also suggest successful attachment of PEG moieties. Evolution of peaks at ~1100 cm^{-1} in PEG-MNP spectra are hallmark indicators of C-O-C ether bond stretching vibrations characteristic of PEG chains [31]. Quantitative barium iodide assay data shown in Table 2 agree with zeta and FTIR results confirming successful synthesis. As illustrated, 5 kDa analogues D5 (4.27 ± 0.68 nmol PEG/mg Fe) and A5 (5.03 ± 0.61 nmol PEG/mg Fe) contained similar PEG labeling as did the 20 kDa analogues D20

(1.14 ± 0.25 nmol PEG/mg Fe) and A20 (1.31 ± 0.04 nmol PEG/mg Fe). Considering the 5-fold difference in molar mass between 5 kDa and 20 kDa NHS-PEG, mass amount of PEG was similar between all PEG-MNPs. Total amine conversion is displayed in Table 2. Both 5 kDa (D5 – 1.45%, A5 – 1.53%) and 20 kDa (D20 – 0.39%, A20 – 0.4%) analogue sets showed similar fractions of amine conversion, suggesting that relative levels of PEG labeling were the same. Amine conversion data also indicate that the vast majority of amine groups on the surface of all candidate PEG-MNPs remain available for additional attachments. Finally, magnetization properties of candidate PEG-MNPs were studied to assess the suitability of the PEG-MNPs for magnetic targeting. Data shown in Figure 3B indicate that magnetic properties of PEG-MNPs are similar to those of aminated precursors. All candidate PEG-MNPs are superparamagnetic (lack of hysteresis) and possess similar saturation magnetization (M) around 100 emu/g Fe—properties comparable to MNPs successfully used in previous magnetic targeting studies [14, 15].

3.3. *In vitro* RES resistance simulations and size stability

As candidate PEG-MNPs were designed to enhance plasma stability and evade elements of the RES, *in vitro* simulations designed to mimic RES processes were performed to predict *in vivo* performance. Specifically, PEG-MNPs were studied with respect to the first two steps (protein binding and subsequent macrophage uptake) of the RES process. To begin, protein binding was measured in 60% FBS at physiologically relevant temperature and pH. As shown in Table 3, D20 protein binding (7.60 ± 0.91 μg/mg Fe) was not statistically different when compared to parent D (6.75 ± 0.96 μg/mg Fe). The lower D5 (5.12 ± 0.42 μg/mg Fe) was statistically different ($p = 0.003$) from D, but the difference was considered small. Both A5 (19.79 ± 1.01 μg/mg Fe, $p < 0.01$) and A20 (20.37 ± 5.28 μg/mg Fe, $p < 0.01$), however, bound about 3–4 fold greater amount of protein than did D/D5/D20.

Next, MNPs were incubated in complete cell culture medium (RPMI 1640 containing 10% FBS and 1% antibiotics) at 37°C over 24 hours to assess both the stability suitability of candidate PEG-MNPs for macrophage uptake studies and also to observe any stability enhancements from PEGylation. The time course for tested MNPs is shown in Figure 4. A and A20 aggregated intensely after suspension in culture medium and were not studied further. Similar to DN, the hydrodynamic diameter of A5 increased ~260 nm immediately and then stabilized for the course of the run. D also increased in size (~300 nm), but much more gradually than did DN or A5. D5 and D20, on the other hand, remained stable throughout the course of the run without any increase in size. From these results, it was determined that A5, D, D5, and D20 were suitable for macrophage uptake studies. PEGylation did appear to confer additional size stability, especially for the D platform. Due to its substantial level of protein binding and instability in cell culture medium, A20 was eliminated from future study. Uptake studies were performed in murine RAW264.7 cells, used commonly to simulate macrophage uptake processes [31,33,38]. Data found in Table 3 indicate that D5 (110 ± 36 fg Fe/cell, $p < 0.001$) and D20 (158 ± 39 fg Fe/cell, $p < 0.001$) uptake was 10 and 7-fold lower respectively when compared to D (1120 ± 97 fg Fe/cell). Despite the improved stability of A5 over precursor A, though, uptake of A5 (11400 ± fg Fe/cell, $p < 0.001$) was about 10-fold higher than D. *In vitro* RES performance studies were promising for D5 and D20 as both exhibited similar protein binding, better stability, and significantly less macrophage uptake when compared to previously targeted D. As a result, D5 and D20 were deemed ready for *in vivo* validation. Based on its significantly higher protein binding and macrophage uptake when compared to D5, D20, and even D, A5 was eliminated from further study.

3.4. Validating enhanced circulation properties of D5 and D20 *in vivo*

Encouraging results for D5 and D20 *in vitro* motivated us to study their potential as long-circulating MNPs *in vivo*. Plasma pharmacokinetic profiles and calculated models are shown in Figure 5 with model parameters shown in Table 4. Variability at each time point is generally low and data appear to follow one-compartment pharmacokinetics. Calculated models all show extremely good fit over the tested time course with $r^2 = 0.99 – 1$. The profile for D particles shows rapid MNP clearance from circulation (CL = 1032 mL/hr/kg, $T_{1/2} = 0.12$ hr), consistent with studies performed previously [15]. In stark contrast, both D5 (CL = 10.15 mL/hr/kg, $T_{1/2} = 7.29$ hr) and D20 (CL = 6.66 mL/hr/kg, $T_{1/2} = 11.75$ hr) were cleared substantially slower. In fact, both D5 and D20 were detectable in circulation through 2.5 days (vs. ~1 hr for D). Calculated V_d is higher for D (185.67 mL/kg) than both D5 (106.89 mL/kg) and D20 (112.95 mL/kg) suggesting greater initial tissue distribution (and out of circulation), likely to be greatest in the liver and spleen [25]. $AUC_{0-\infty}$ represents the total expected plasma exposure from a single dose (12 mg Fe/kg) of MNPs. As shown in Table 4, calculated $AUC_{0-\infty}$ values for D5 (1182 μg Fe * hr/mL) and D20 (1801 μg Fe * hr/mL) were two orders of magnitude higher than for D (12 μg Fe * hr/mL).

Brain tumors are often positioned deep within the skull, away from the body surface, where applied field gradients drop off substantially. As this effect might be partially minimized with the targeting of a long-circulating MNP, a brain tumor was considered a good model to visually validate the pharmacokinetic results above. As shown in Figure 6, tumors are identified on T_2-weighted images as hyperintense regions within the brain. MNPs are strong enhancers of T_2/T_2* proton relaxation and are, thus, identified as hypointense (negative contrast) regions on T_2*-weighted GE MRI scans. The GE brain scan obtained after administration of D shows negligible presence, which would be observed as hypointensity in the tumor (or brain) throughout the course of the run. This observation is consistent with results obtained previously [14]. Conversely, dynamic scans of animals exposed to D5 and D20 show sustained signal reduction in both the brain (evidenced by clear delineation of brain fissures compared to baseline) and even more so in the tumor (likely due to the highly vascular nature of solid tumors), consistent with GE brain scans of other longer-circulating MNPs [23]. In fact, some hypointensity can be observed in D5 and D20 GE scans even at 24 hours. Sustained negative contrast in both the brain and tumor over time visually confirm that D5 and D20 are indeed long circulating and, as a result, better exposed to the tumor.

4. DISCUSSION

The ideal MNP platform for magnetically targeted tumor therapy would possess a large (> 100 nm), superparamagnetic core suitable for magnetic capture and retention; contain functionality to couple therapeutic cargoes/additional targeting ligands; be non-toxic; and show long-circulating behavior. As was discussed previously, pharmacokinetics are as important as nanoparticle physical properties and magnet setup when it comes to targeting success—magnetic targeting *depends* on sustained circulation delivery of MNPs to targeted tumors. Targeting favors increased particle sizes that stem from larger cores, but larger sizes increase the visibility of MNPs to the RES resulting in faster clearance times. Functionalization of MNPs can also compete with pharmacokinetics, a good example illustrated by the nearly instant plasma clearance of highly cationic (e.g. polyethyleneimine (PEI) grafted) MNPs [15]. Considering the above requirements and shortcomings of the status quo, this work strived to develop long-circulating, functionalized MNPs suitable for magnetic tumor targeting.

PEG has been deemed an answer to many pharmacokinetic problems related to fast clearance as it resists RES elements, and therefore, was used in this work. PEG is generally considered non-toxic and is also useful in acting as a stabilizer in otherwise destabilizing

environments that include less-than-favorable synthesis conditions. It was recently reported that PEGylation of MNPs can be challenging and requires many complicated steps that can involve organic phases [22]. Our PEGylation procedure using NHS chemistry was easy and could be completed using commercially available agents in aqueous phases. Also important, PEGylation did not substantially change particle sizes, morphology, or magnetic properties (Figures 2 & 3, Table 2) maintaining nanoparticle suitability for magnetic targeting. PEGylation procedures were carefully controlled so that molar levels of PEG labeling (Table 2) were similar for 5 kDa and 20 kDa analogues between A and D platforms and similar across all candidates with respect to mass. Similar PEG contents permitted us to make performance inferences with respect to type of nanoparticle coat (simple small organic linker vs. a cross-linked macromolecular polysaccharide coating) and organization of PEG on the surface (shorter PEG chains in greater surface density vs. longer PEG chains with less surface density). Regardless of the molecular weight of PEG used, >98% (Table 2) of the measured amine groups in Table 1 were still available for additional syntheses on MNP surfaces. These groups would likely prove useful in coupling other cargoes, such as therapeutic moieties and/or other PEG modified with additional targeting ligands. Moreover, amine groups (cationic in nature) reside at the surface of the MNP, which, as was shown here, were shielded by PEG chains, rendering them relatively inert to otherwise fast clearing mechanisms. At the conclusion of syntheses and characterization, all candidate MNPs appeared suitable for magnetic targeting *and* suitable for therapeutic/targeting ligand attachments.

We first used simulations designed to mimic RES processes and size stability in a complex medium to predict the circulation behavior of candidate PEG-MNPs *in vitro*. These *in vitro* experiments provided valuable insight to the importance of coating type (prior to PEGylation) on general stability and resistance to the RES. Particle size stability measurements made in complete cell culture medium at 37°C (Figure 4) clearly sugg est that sufficient PEGylation of either platform improved stability shown by the lack of intense aggregation by A5 MNPs compared to parent A, which aggregated immediately. Sustained stability (no measureable size increases) was observed for both D5 and D20, compared to parent D, which gradually increased in size over the course of the run. In addition to stability enhancements from PEGylation across both platforms, size experiments suggest that the more durable cross-linked starch coating of D5 and D20 synergizes with its attached PEG moieties to impart even better nanoparticle stability. This hypothesis is evidenced by the fact that neither A5 nor A20 (possessing no macromolecular coating) showed sustained stability over the course of the run, despite possessing a similar PEG content to D5 and D20 respectively. Observations from protein binding studies (Table 3) suggest that a more durable coating might also help in exerting resistance to the RES. Both A5 and A20 showed significantly higher protein binding than D5 or D20, and even previously targeted D. Interestingly, little difference in protein binding was observed across the starch-based species. Differences between D5/D20 and parent D were observed, though, in macrophage uptake studies. As was the case with size stability and protein binding experiments, significantly greater macrophage uptake was observed for A5 when compared to D5/D20 (~100-fold), and D (~10-fold). D5 and D20, however, showed a 7 to 10-fold reduction in macrophage uptake, suggesting that D5 and D20 might remain in plasma longer than previously targeted D. Uptake data again demonstrate the important observed synergy of the cross-linked starch coating and its attached PEG, which appeared likely to better resist macrophage sequestration *in vivo*. As A5 and A20 generally performed at or worse than D *in vitro*, they were not expected to show enhanced circulation times and were, thus, not considered *in vivo*.

Considering our promising results with D5 and D20 *in vitro*, *in vivo* studies were essential. Much to our surprise, D5 (7.29 hr) and D20 (11.75 hr) showed 61- and 98-fold greater

calculated plasma half-lives in rats respectively than previously targeted parent D (0.12 hr). In fact, despite a 7–8 times greater hydrodynamic size, our reported plasma half-lives for D5 and D20 are 2.2–3.6 times longer than that (3.3 hr in rats) reported for 20 nm Clariscan (feruglose) MNP, coated with PEGylated, oxidized starch [39]. The longer PEG chain lengths of D20 did appear to produce longer circulating MNPs than the more densely packed, shorter chains on D5. A difference in circulation residence due to surface PEG arrangement was an interesting find considering the lack of substantial differences between D5 and D20 during protein binding and macrophage uptake simulations. Higher plasma residence resulted in higher total exposure of plasma to D5 and D20 illustrated by calculated $AUC_{0\text{-}\infty}$ values in Table 4 and images in Figure 6. It has been shown that arterial plasma $AUC_{0\text{-}\infty}$ is directly proportional to the $AUC_{0\text{-}\infty}$ of a tissue compartment supplied by arterial blood [40]. If it is assumed that the plasma concentration of D5 or D20 in intravenous blood is similar to the concentration in arterial blood supplying a tumor at any given time (due to slow MNP clearance), it is estimated that 100 to 150 times greater MNP exposure would be achieved for tumors exposed to D5 and D20 respectively when compared to previously targeted D. Two orders of magnitude higher tumor exposures to MNPs could greatly enhance the efficiency of magnetic tumor targeting as long-circulating MNPs could be presented to tumors many times over, increasing the probability of magnetic capture when combined with prolonged targeting times. This advantage would be especially beneficial for tumors positioned away from the body surface (e.g. brain), where magnetic gradient strengths are known to drop off exponentially [19]. MR images (Figure 6) clearly showing sustained exposure of brain tumors to MNPs are a testament to that conjecture. It should also be noted that images were taken from animals intravenously administered with D5 and D20, the route clearly preferred by patients and physicians in clinical practice—no additional interventions were required.

For the first time, we report a PEG modified, cross-linked starch coated MNPs specifically designed for enhanced magnetic tumor targeting. D5 and D20 are easily produced from commercially available materials; possess physical and magnetic properties suitable for magnetic targeting; are amine functionalized for attachment of additional cargoes (e.g. therapeutic & other targeting moieties); and possess sufficiently long plasma residence rendering both attractive platforms for magnetically targeted tumor therapy. Cross-linked starch coatings and attached PEG appear to work synergistically in exerting resistance to the RES, thus, promoting longer plasma residence. D5 and D20 are made of non-toxic components and do clear from plasma eventually, suggesting favorable toxicity profiles—though, more studies are needed to validate that claim. In particular, future biodistribution studies of D5 and D20 will be valuable in understanding both total body clearance and the extent of targeting enhancements in specific tumor models.

5. CONCLUSION

Commercially available starch coated MNPs were cross-linked, aminated, and modified with PEG (5 kDa and 20 kDa molecular weights) using NHS chemistry to produce long-circulating PEG-MNPs suitable for magnetic tumor targeting. The end products (D5 and D20) possessed 61–98 fold longer plasma half-life (on the order of hours instead of minutes) in rats than unmodified starch MNPs – an MNP typical of those used in previous magnetic tumor targeting attempts. Enhanced plasma residence resulted in 100–150 greater tumor exposures to MNPs after intravenous administration. The observed pharmacokinetic advantages of D5 and D20 justify future studies in magnetically targeted tumor models.

Acknowledgments

This work was supported in part by National Institutes of Health (NIH) R01 Grants CA114612, NS066945, and a Hartwell Foundation Biomedical Research Award. This work was also partially sponsored by Grant R31-2008-000-10103-01 from the WCU project of South Korea. Victor C. Yang is currently a participating faculty member in the Department of Molecular Medicine and Biopharmaceutical Sciences, Seoul National University, South Korea. Adam Cole is the recipient of a NIH Pharmacological Sciences and Bio-related Chemistry Training Grant (GM007767 from NIGMS), a University of Michigan Rackham Pre-Doctoral Fellowship, and is currently an American Foundation for Pharmaceutical Education (AFPE) Pre-Doctoral Fellow. The authors would like to thank Dr. Christian Bergemann and Dr. Rainer Quaas of Chemicell, GmbH for their unwavering technical assistance with respect to MNPs. We would also like to thank Jim Windak for help with FTIR/ESR, Dr. Beata Chertok for assistance with animal techniques, and Amanda Welton of the UM Center for Molecular Imaging for additional animal suggestions and technical assistance with MRI.

References

1. Goya GF, Grazu V, Ibarra MR. Magnetic nanoparticles for cancer therapy. Curr Nanosci 2008;4:1–16.
2. McBain SC, Yiu HHP, Dobson J. Magnetic nanoparticles for gene and drug delivery. Int J Nanomed 2008;3:169–80.
3. Yu Y, Sun D. Superparamagnetic iron oxide nanoparticle ‘theranostics’ for multimodality tumor imaging, gene delivery, targeted drug and prodrug delivery. Expert Review of Clinical Pharmacology 2010;3:117–30.
4. Ferrari, M.; Lee, AP.; Lee, LJ.; Josephson, L. BioMEMS and Biomedical Nanotechnology. Springer; US: 2006. Magnetic nanoparticles for MR imaging; p. 227-37.
5. Jordan A, Scholz R, Maier-Hauff K, van Landeghem FKH, Waldoefner N, Teichgraeber U, et al. The effect of thermotherapy using magnetic nanoparticles on rat malignant glioma. J Neuro-Oncol 2006;78:7–14.
6. Peng XH, Qian XM, Mao H, Wang AY, Chen Z, Nie SM, et al. Targeted magnetic iron oxide nanoparticles for tumor imaging and therapy. Int J Nanomed 2008;3:311–21.
7. McCarthy JR, Weissleder R. Multifunctional magnetic nanoparticles for targeted imaging and therapy. Adv Drug Deliv Rev 2008;60:1241–51. [PubMed: 18508157]
8. Maeda H. Tumor-selective delivery of macromolecular drugs via the EPR effect: background and future prospects. Bioconjugate Chem 2010;21:797–802.
9. Sonvico F, Mornet S, Vasseur S, Dubernet C, Jaillard D, Degrouard J, et al. Folate-conjugated iron oxide nanoparticles for solid tumor targeting as potential specific magnetic hyperthermia mediators: synthesis, physicochemical characterization, and in vitro experiments. Bioconjugate Chem 2005;16:1181–8.
10. Yallapu MM, Foy SP, Jain TK, Labhasetwar V. PEG-functionalized magnetic nanoparticles for drug delivery and magnetic resonance imaging application. Pharm Res 2010;27:2283–95. [PubMed: 20845067]
11. Veiseh O, Sun C, Fang C, Bhattarai N, Gunn J, Kievit F, et al. Specific targeting of brain tumors with an optical/magnetic resonance imaging nanoprobe across the blood-brain barrier. Cancer Res 2009;69:6200–7. [PubMed: 19638572]
12. Dobson J. Magnetic nanoparticles for drug delivery. Drug Dev Res 2006;67:55–60.
13. Alexiou C, Jurgons R, Seliger C, Brunke O, Iro H, Odenbach S. Delivery of superparamagnetic nanoparticles for local chemotherapy after intraarterial infusion and magnetic drug targeting. Anticancer Res 2007;27:2019–22. [PubMed: 17649815]
14. Chertok B, Moffat BA, David AE, Yu FQ, Bergemann C, Ross BD, et al. Iron oxide nanoparticles as a drug delivery vehicle for MRI monitored magnetic targeting of brain tumors. Biomaterials 2008;29:487–96. [PubMed: 17964647]
15. Chertok B, David AE, Yang VC. Polyethyleneimine-modified iron oxide nanoparticles for brain tumor drug delivery using magnetic targeting and intra-carotid administration. Biomaterials 2010;31:6317–24. [PubMed: 20494439]
16. Dobson J. Gene therapy progress and prospects: magnetic nanoparticle-based gene delivery. Gene Ther 2006;13:283–7. [PubMed: 16462855]

17. Jurgons R, Seliger C, Hilpert A, Trahms L, Odenbach S, Alexiou C. Drug loaded magnetic nanoparticles for cancer therapy. J Phys-Condes Matter 2006;18:S2893–S902.
18. Gupta AK, Gupta M. Synthesis and surface engineering of iron oxide nanoparticles for biomedical applications. Biomaterials 2005;26:3995–4021. [PubMed: 15626447]
19. Liu HL, Hua MY, Yang HW, Huang CY, Chu PC, Wu JS, et al. Magnetic resonance monitoring of focused ultrasound/magnetic nanoparticle targeting delivery of therapeutic agents to the brain. Proc Natl Acad Sci U S A 2010;107:15205–10. [PubMed: 20696897]
20. Radermacher KA, Beghein N, Boutry S, Laurent S, Elst LV, Muller RN, et al. In vivo detection of inflammation using pegylated iron oxide particles targeted at E-selectin: a multimodal approach using MR imaging and EPR spectroscopy. Invest Radiol 2009;44:398–404. [PubMed: 19554667]
21. Larsen EKU, Nielsen T, Wittenborn T, Birkedal H, Vorup-Jensen T, Jakobsen MH, et al. Size-dependent accumulation of PEGylated silane-coated magnetic iron oxide nanoparticles in murine tumors. ACS Nano 2009;3:1947–51.
22. Sun CR, Du K, Fang C, Bhattarai N, Veiseh O, Kievit F, et al. PEG-mediated synthesis of highly dispersive multifunctional superparamagnetic nanoparticles: their physicochemical properties and function in vivo. ACS Nano 2010;4:2402–10. [PubMed: 20232826]
23. Moffat BA, Reddy GR, McConville P, Hall DE, Chenevert TL, Kopelman RR, et al. A novel polyacrylamide magnetic nanoparticle contrast agent for molecular imaging using MRI. Mol Imaging 2003;2:324–32. [PubMed: 14717331]
24. Tromsdorf UI, Bruns OT, Salmen SC, Beisiegel U, Weller H. A highly effective, nontoxic T1 MR contrast agent based on ultrasmall PEGylated iron oxide nanoparticles. Nano Lett 2009;9:4434–40. [PubMed: 19799448]
25. Chertok B, Cole AJ, David AE, Yang VC. Comparison of electron spin resonance spectroscopy and inductively-coupled plasma optical emission spectroscopy for biodistribution analysis of iron-oxide nanoparticles. Mol Pharm 2010;7:375–85. [PubMed: 20039679]
26. Pittet MJ, Swirski FK, Reynolds F, Josephson L, Weissleder R. Labeling of immune cells for in vivo imaging using magnetofluorescent nanoparticles. Nat Protoc 2006;1:73–9. [PubMed: 17406214]
27. Hamdi G, Ponchel G. Enzymatic degradation of epichlorohydrin crosslinked starch microspheres by alpha-amylase. Pharm Res 1999;16:867–75. [PubMed: 10397607]
28. Moore S, Stein WH. Photometric ninhydrin method for use in the chromatography of amino acids. J Biol Chem 1948;176:367–88. [PubMed: 18886175]
29. Skoog B. Determination of polyethylene glycol-4000 and glycol-6000 in plasma-protein preparations. Vox Sang 1979;37:345–9. [PubMed: 44395]
30. Mu QX, Li ZW, Li X, Mishra SR, Zhang B, Si ZK, et al. Characterization of protein clusters of diverse magnetic nanoparticles and their dynamic interactions with human cells. J Phys Chem C 2009;113:5390–5.
31. Xie J, Xu C, Kohler N, Hou Y, Sun S. Controlled PEGylation of monodisperse Fe3O4 nanoparticles for reduced non-specific uptake by macrophage cells. Adv Mater 2007;19:3163–6.
32. Ross BD, Zhao YJ, Neal ER, Stegman LD, Ercolani M, Ben-Yoseph O, et al. Contributions of cell kill and posttreatment tumor growth rates to the repopulation of intracerebral 9L tumors after chemotherapy: An MRI study. Proc Natl Acad Sci U S A 1998;95:7012–7. [PubMed: 9618530]
33. Zhang Y, Kohler N, Zhang MQ. Surface modification of superparamagnetic magnetite nanoparticles and their intracellular uptake. Biomaterials 2002;23:1553–61. [PubMed: 11922461]
34. Flesch C, Unterfinger Y, Bourgeat-Lami E, Duguet E, Delaite C, Dumas P. Poly(ethylene glycol) surface coated magnetic particles. Macromol Rapid Commun 2005;26:1494–8.
35. Herve K, Douziech-Eyrolles L, Munnier E, Cohen-Jonathan S, Souce M, Marchais H, et al. The development of stable aqueous suspensions of PEGylated SPIONs for biomedical applications. Nanotechnology 2008;19:465608.
36. Jiang JS, Gan ZF, Yang Y, Du B, Qian M, Zhang P. A novel magnetic fluid based on starch-coated magnetite nanoparticles functionalized with homing peptide. J Nanopart Res 2009;11:1321–30.
37. Mahato, RI. Biomaterials for delivery and targeting of proteins and nucleic acids. Boca Raton: CRC Press; 2005.

38. Wuang SC, Neoh KG, Kang ET, Pack DW, Leckband DE. Heparinized magnetic nanoparticles: in-vitro assessment for biomedical applications. Adv Funct Mater 2006;16:1723–30.

39. Preda A, van Vliet M, Krestin GP, Brasch RC, van Dijke CF. Magnetic resonance macromolecular agents for monitoring tumor microvessels and angiogenesis inhibition. Invest Radiol 2006;41:325–31. [PubMed: 16481916]

40. Eckman WW, Patlak CS, Fensterm Jd. Critical evaluation of principles governing advantages of intra-arterial infusions. J Pharmacokinet Biopharm 1974;2:257–85. [PubMed: 4452940]

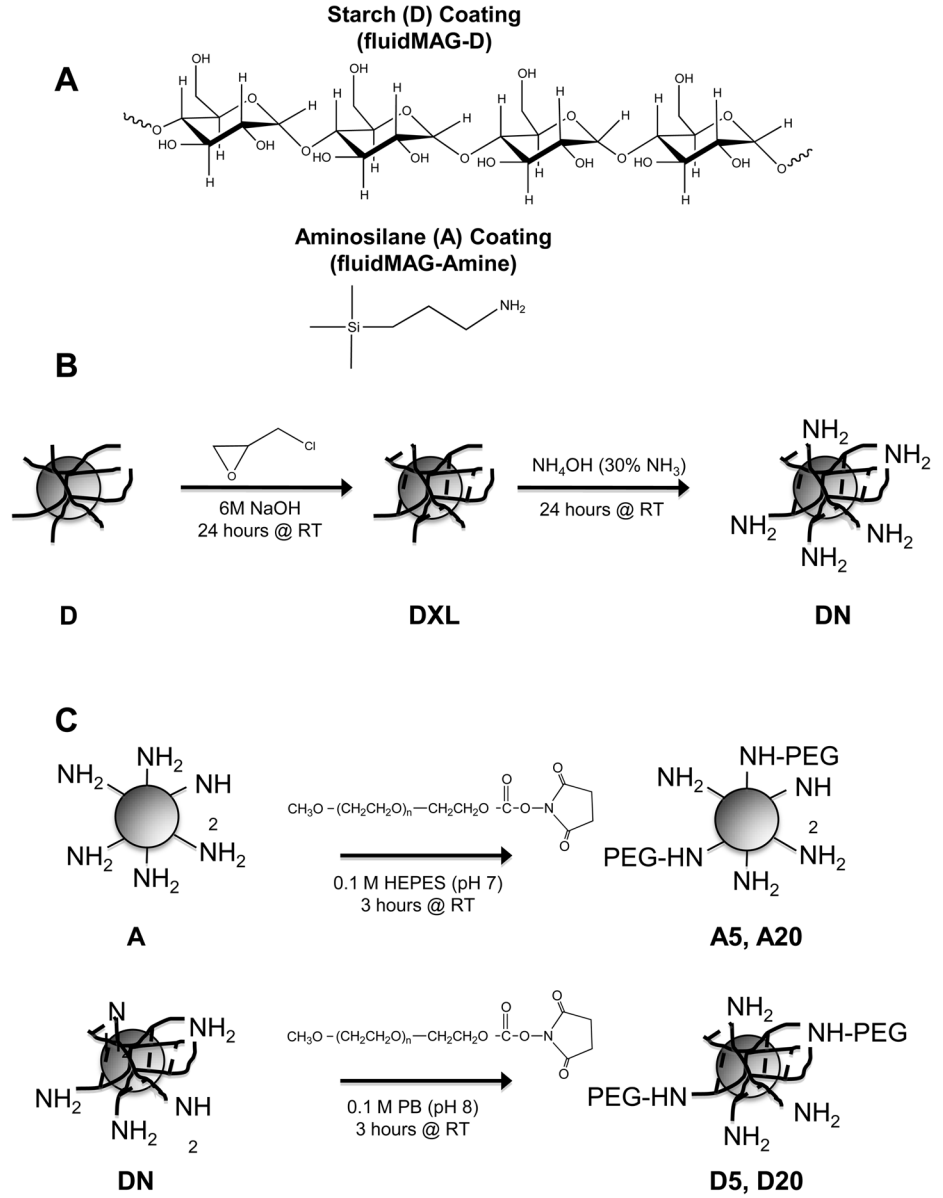

Figure 1.

(**A**) Molecular representations of starch and aminosilane coatings of fluidMAG-D (D) and fluidMAG-Amine (A) respectively. Starch hydroxyl groups of D provide anchor points for attachments to the polysaccharide coating, whereas amine groups of A provide anchor points for attachments directly to the iron oxide core. (**B**) Synthesis strategy for strengthening (cross-linking) the starch coating on D to produce DXL. Subsequent amine functionalization produces DN. Amination of DXL renders it functionally similar to A. (**C)** Synthesis strategy for PEG-MNP candidates. N-Hydroxysuccinimide (NHS) chemistry is used to link PEG to aminated precursors. Methoxyl PEG succinimidyl carbonate (SC) ester was used in conjugations as it has substantially better stability (yet, retains reactivity) than more commonly sold methoxyl PEG succinimidyl carboxylmethyl ester (SCM). 5 kDa and 20 kDa molecular weight NHS-PEGs were used to produce 5 kDa (A5, D5) and 20 kDa (A20, D20) PEG-MNP analogues for each aminated precursor MNP (A, DN).

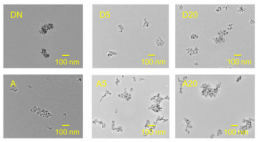

Figure 2.
TEM micrographs of PEG and aminated precursor MNPs (Magnification 20000x). Images show that the morphology of MNPs is conserved through syntheses, with MNPs possessing cores of clustered iron-oxide domains—a feature critical for magnetic targetability. Micrographs also generally agree with MNP size and polydispersity measurements made with DLS.

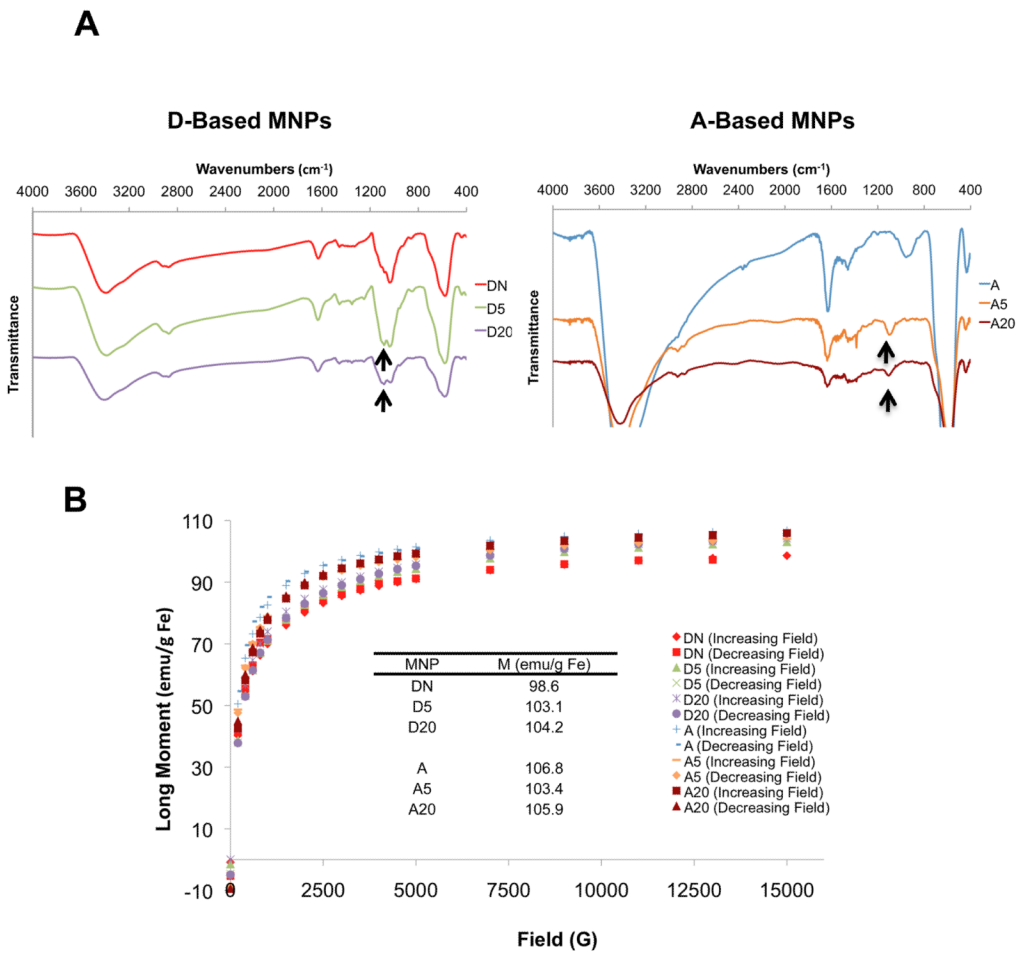

Figure 3.

(**A**) FTIR spectra of lyophilized PEG and aminated precursor MNP powders. Stretches at ~1100 cm^{-1} (indicated by arrows) in PEG-MNP spectra are characteristic ether (C-O-C) bond stretches that confirm successful PEGylation. (**B**) Magnetization properties of PEG and aminated MNPs from SQUID analyses. Data show that PEG-MNPs are superparamagnetic (no hysteresis); that PEG-MNP candidates all possess similar saturation magnetization (M - shown in the inset table); and that synthesis procedures do not alter PEG-MNP magnetics from precursors.

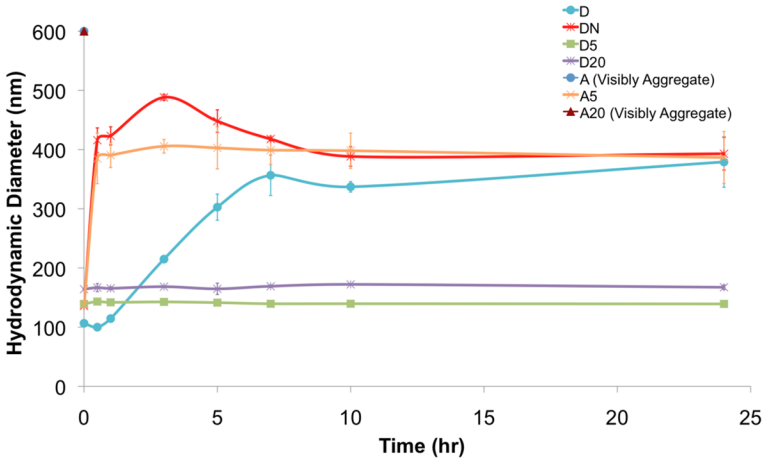

Figure 4.

Particle size stability time-course in complete cell culture medium (RPMI 1640 containing 10% FBS+1% antibiotics, n = 3) at 37°C. A and A20 v isually aggregated immediately after suspension in culture medium and were not studied further. A5, while increasing in size some, did exhibit improved stability over precursor A. Both D5 and D20, however, remained stable over the entire course of the run, outperforming unmodified D and also A5.

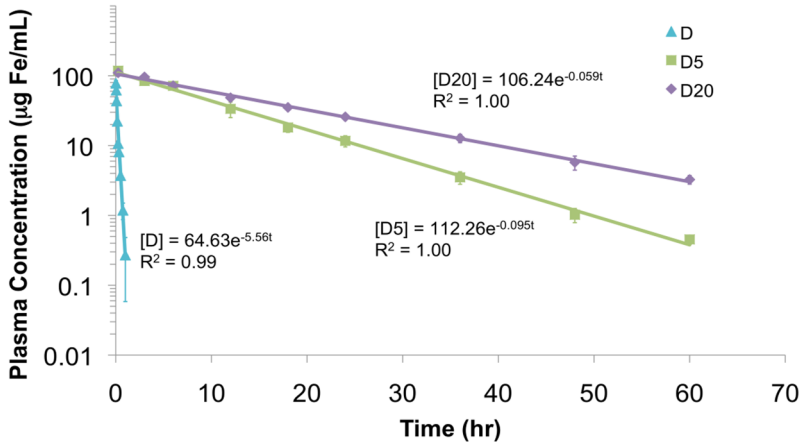

Figure 5.

Plasma pharmacokinetic analysis of D5, D20, and previously targeted D in Male Fisher 344 rats (12 mg Fe/kg, ~200g animal). Data clearly indicate that D5 and D20 possess substantially longer plasma residence when compared to D. Data for each MNP appear to follow a one-compartment model and non-linear regression was used to calculate the model equation shown next to each data set. Pharmacokinetic parameters were extracted/calculated from models and are shown in Table 4.

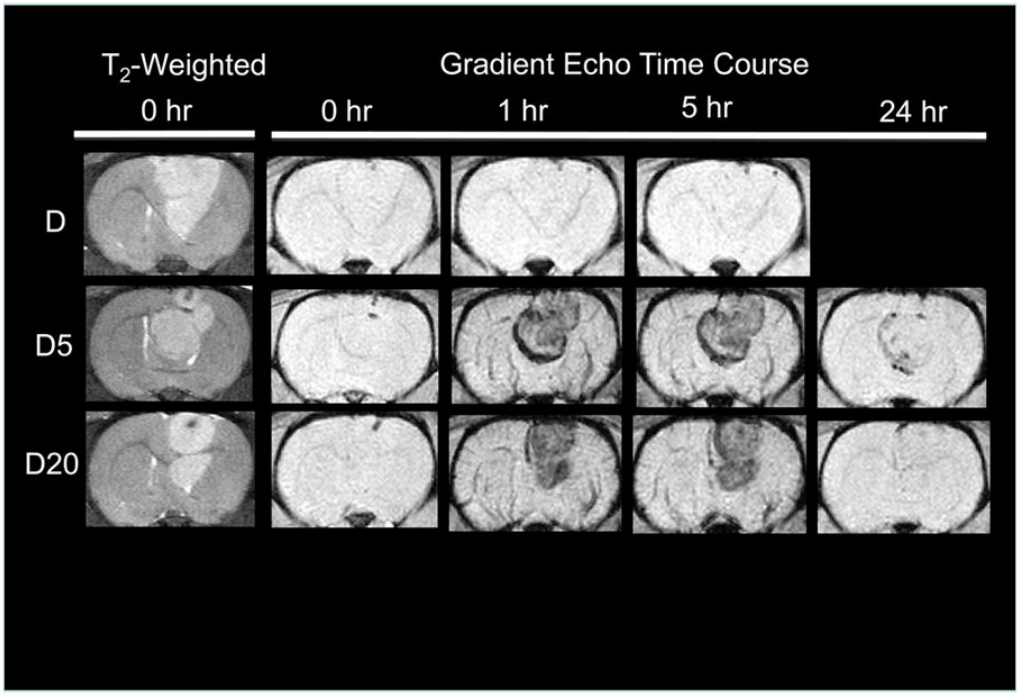

Figure 6.

Representative MRI time course in male Fisher 344 rats bearing 9L glioma brain tumors (12 mg Fe/kg, ~200g animal). Baseline T_2-weighted, fast spin echo images clearly indicate the positioning of the tumor (hyperintense region) in the brain. T_3*-weighted, gradient echo images provide qualitative information about MNP presence in the brain/tumor. Sustained negative contrast (hypointensity) in both tumor and normal brain through five hours substantiates the pharmacokinetic data in Figure 5/Table 4, visually confirming that D5 and D20 reside far longer in plasma and are exposed to tumor when compared to D. In fact, hypointensity can still be observed in tumors through 24 hours.

Table 1

Characterization of D, and aminated precursor MNPs, DN & A

MNP	Hydrodynamic Diameter (nm)	PDI	Zeta Potential (mV)	[NH_2] (nmol/mg Fe)
D	104.1 ± 2.3	0.073	+9.0 ± 0.8	-
DN	134.3 ± 2.1	0.058	+58.9 ± 0.6	293 ± 32
A	114.2 ± 1.2	0.151	+54.6 ± 0.8	329 ± 29

Samples measured very dilute in DI H_2O @ 25°C for DLS measurements

Ninhydrin assay used to determine [NH_2]

For all experiments, n = 3

Table 2

Characterization of candidate PEG-MNPs

MNP	Hydrodynamic Diameter (nm)	PDI	Zeta Potential (mV)	[PEG] (nmol/mg Fe)	% NH_2 conversion
DN	134.3 ± 2.1	0.058	+58.9 ± 0.6	-	-
D5	142.2 ± 5.6	0.045	+24.4 ± 1.0	4.27 ± 0.68	1.45
D20	168.5 ± 1.4	0.024	+25.6 ± 0.4	1.14 ± 0.25	0.39
A	114.2 ± 1.2	0.151	+54.6 ± 0.8	-	-
A5	151.5 ± 1.6	0.164	+25.7 ± 0.3	5.03 ± 0.61	1.53
A20	190.0 ± 5.8	0.115	+25.4 ± 0.4	1.31 ± 0.04	0.4

Samples measured very dilute in DI H_2O @ 25°C for DLS determinations

Barium iodide assay used to determine [PEG]

For all experiments, n = 3

Table 3

In vitro RES simulation results

MNP	Protein Binding (μg/mg Fe)	RAW264.7 Uptake (fg Fe/cell)
D	6.75 ± 0.96	1120 ± 97
D5	5.12 ± 0.42*	110 ± 36**
D20	7.60 ± 0.91	158 ± 39**
A5	19.79 ± 1.01*	11400 ± 1700**
A20	20.37 ± 5.28*	Not Tested

* ($p < 0.01$),

** ($p < 0.001$)

For both studies, n = 6

Table 4

Calculated parameters obtained from experimentally determined pharmacokinetic model

MNP	C_0 (μg Fe/mL)	*k* (1/hr)	$T_{1/2}$ (hr)	Vd (mL/kg)	CL (mL/hr/kg)	$AUC_{0-\infty}$ (μg Fe * hr/mL)
D	64.63	5.560	0.12	185.67	1032	12
D5	112.26	0.095	7.29	106.89	10.15	1182
D20	106.24	0.059	11.75	112.95	6.66	1801

Dose (200 g animal) = 2400 μg Fe

Biomaterials. Author manuscript; available in PMC 2012 March 1.